MET.O.14

METEOROLOGICAL OFFICE
BOUNDARY LAYER RESEARCH BRANCH
TURBULENCE & DIFFUSION NOTE

T.D.N. No. 97

Direct Measurements of the Energy Balance over a Grass Surface - A Preliminary Report.

by

C.J.Richards

November 1978

Direct Measurements of the Energy Balance over a Grass Surface - A Preliminary Report

by C J Richards

Summary

Since the spring of 1976 an experiment has been in progress at the Meteorological Research Unit, RAF Cardington, designed to measure directly the components in the energy budget over a grass surface, and to study their variation over time scales ranging from one hour to several months. The instrumentation used in this experiment is described, and some theoretical background presented. Measurements made during the spring and summer of 1976 show that the energy budget is capable of changing significantly over periods as short as a few hours. Evaporation, in particular, is found to exert a very strong influence on the energy budget.

1. Introduction

Much attention has been paid recently to the problem of describing and modelling the atmospheric boundary layer; see, for example, Smith and Carson (1974). In particular, attempts have been made to describe the behaviour of the surface boundary layer in terms of external, readily assessed physical and meteorological parameters; eg Smith (1975). The surface boundary layer, which comprises the lowest few tens of metres of the atmosphere, is that layer directly influenced by the underlying surface and in which the turbulent fluxes of momentum, heat, and water vapour vary by only a small percentage from their surface values. It is a very important region of the atmosphere because, not only are man's activities largely confined to it, but also many of the basic energy transformations occur within it. On a clear day, for instance, incoming solar radiation is

absorbed at the earth's surface, and converted into radiant energy of longer wavelength and also into other forms of heat energy. How this conversion occurs depends very much upon the nature of the surface. For a typically vegetated land surface the net incident radiation is converted into (a) latent heat of evaporation, and (b) ordinary (or "sensible") heat. Some of this sensible heat is conducted down into the ground as a soil heat flux, and the rest is used to heat the overlying air through a combination of eddy diffusion, radiative, and molecular conduction processes. The balance struck between these energy components will vary from one surface to another, and can also change daily over a given surface. Small scale motion systems in the atmosphere are strongly influenced by the nature of the underlying surface; for instance, cumulus convection, the sea breeze and heat thunderstorm, or radiation fog - and this influence becomes stronger as the scale decreases. It is therefore logical to presume that any attempt to understand these systems would be incomplete without a knowledge of the energy budget at the surface.

Despite theoretical attempts to do so there have been, until recently, few attempts at measuring directly the components of the surface energy budget over a prolonged period. Blackwell (1963) has described some experimental work at Cambridge in wh ich measurements were made to assess the importance of evaporation in the energy budget. However, in an experiment at the Meteorological Research Unit, Cardington, the energy balance components over a grassy site have been measured since 1976. This paper forms a general introduction to this experiment and presents some of the data that was collected during the spring and summer of 1976.

2. Definition of the Energy Balance Equation

From the principle of conservation of energy it is clear that all gains and losses of energy at the earth's surface must balance. For a uniform, horizontal land surface this balance can be expressed by the equation:

$$R_N = H + G + LE \qquad (1)$$

where R_N is the net receipt of radiant energy at the surface, H is the flux of sensible heat transferred from the surface to the air above it, G is the downward flux of heat into the soil, and LE is the energy required to evaporate surface moisture; (see Munn, 1966). R_N represents the radiation balance among the following components (refer to Fig. 1):

Q_1 = direct, shortwave radiation - the solar beam;

Q_2 = diffuse, shortwave radiation - scattered from clouds and the atmosphere;

Q_3 = shortwave radiation scattered by the surface - upward;

Q_4 = longwave emission from the atmosphere - downward; and

Q_5 = longwave emission from the ground - upward.

Therefore $$R_N = Q_1 + Q_2 + Q_4 - Q_3 - Q_5 \qquad (2)$$

By convention, positive R_N represents a net gain (or warming), and negative R_N a net loss (or cooling) of radiant energy. Positive H defines the heat energy available for warming the air, and it is associated with an unstable temperature stratification in the surface layer, ie $d\theta/dz < 0$. Negative H defines the downward heat flux through a stable layer, ie where $d\theta/dz > 0$. $G > 0$ represents the downward soil heat flux which arises when the temperature of the soil decreases with depth. $G < 0$ describes the upward flux of heat generated by the reversal of this temperature gradient. Positive

LE defines the upward transfer of water vapour into the overlying air through evaporation, and constitutes the latent heat flux. $LE < 0$ defines condensation, such as dewfall. The latent heat flux is related to the rate of evaporation E through the equation

$$LE = E \times L_v \qquad (3)$$

where L_v is the latent heat of vaporization.

For a vegetation-covered surface LE strictly represents the energy loss due both to evaporation of surface moisture and the transpiration of water vapour from the vegetation cover itself. In this respect, LE defines the net water loss, or "evapotranspiration", from the surface. "Potential evapotranspiration" is the evaporation from a vegetation cover that is never short of water. In practice, the actual evaporation, as defined by LE, depends very much upon the available water in the ground, and if the reserves of soil moisture are not regularly replenished by rainfall, LE can fall very quickly below the equivalent potential rate of evapotranspiration; see Penman (1949). In this respect, the moisture available in the ground exerts as important an influence on LE as does the atmosphere. (A review of the physics of evaporation is given by Penman, 1956).

The components of the energy balance are defined in terms of their flux intensities, using watts per square metre (Wm^{-2}). For comparison purposes, the solar constant $S = 1400\ Wm^{-2}$.

MEASUREMENT OF THE SURFACE ENERGY BUDGET - INSTRUMENTATION

3. The Experimental Site

The experimental site at Cardington lies about 4 km southeast of Bedford within the broad clay vale of the River Ouse. It provides an excellent exposure to the weather from most directions. There are, however, two large hangars (approx 50 m high) about 0.5 km

to the north, and the outer suburbs of Bedford lie about 2 km to the northwest. Both the site and its immediate surroundings are grass-covered, but the surface of the agricultural land beyond varies from arable and cereal cover to rough pasture and small woods. The fetch over grass is limited to between 400 and 800 m, and this restricts the constant flux layer at the site to a depth of little more than 4 m. A plan view of the instrument enclosure at Cardington is given in Fig. 2.

4. Measurement of Net Radiation and Soil Heat Flux

The net radiation, R_N in equation (1), is measured directly with a ventilated radiation balance meter of the Kew Observatory pattern, supported parallel to the surface at a height of around 1 m. The sensing element is a thermopile which is embedded in a blackened plate, and measurements are accurate to between 5 and 10 per cent. The calibration of the instrument is checked at approximately six monthly intervals. Useful measurements cannot be made when it is raining.

The soil heat flux G at the surface ($z = 0$) is an extrapolated estimate based upon measurements at several levels below the surface. This is because it is physically impossible to measure this quantity without disturbing the surface. Furthermore, not only does the finite size of the sensor produce an unavoidable volume-integrated measurement, but also the sensor must be buried deep enough to prevent any direct sky or solar radiation reaching it. An alternative approach to the problem would be to measure the soil temperature profile with small thermo-electric sensors, and to calculate the heat flux through the soil using the equation of thermal conductivity. Unfortunately, the conductivity coefficient in soil can vary greatly

with depth since it depends on density and moisture content in the soil, and these variations are often exaggerated in the surface layers; see, for example, Geiger (1950). An amenable solution is to use suitably calibrated flux plates, and this approach has been adopted in this experiment. Five flux plates were buried in a hole at depths of 5, 10, 20, 40 and 80 cm (Fig. 3), with the top plate lying in contact with the root system of the thick turf cover on the surface. Care was taken to ensure that the soil removed from the hole before the plates were buried was replaced at approximately the same depth afterwards. A second, shallower hole was dug about 20 m away, and two plates installed at 5 cm and 10 cm for comparison purposes. The estimate of G is based upon extrapolation of measurements at 5, 10 and 20 cm depth, and confidence in this quantity is limited to 20 per cent; although it probably exceeds 50 per cent on clear days when the flux divergence in the top 10 cm of soil is particularly large, as is likely when R_N is changing rapidly with time.

5. Measurement of Latent Heat Flux

Evaporation measurements are made routinely at Cardington, independently of the experimental programme. Evaporation from a water surface is measured daily using a Met Office British standard evaporation tank. The latent heat flux, LE, is derived from hourly measurements of the evapotranspiration from the short-cropped grass surface of a weighing lysimeter; (see Blackwell, 1963). This is a square tank of surface area 2 m^2 and depth 50 cm, and it contains a sample of soil representative of the surrounding site. The change in the weight of this tank due to evaporation from the surface or rainfall upon it is monitored automatically. If Δh mm is the

equivalent depth of water evaporated from the surface of the lysimeter during a period Δt sec, the rate of evaporation E per unit area is given by

$$E = \frac{\Delta h}{\Delta t} \text{ kgm.sec}^{-1} \text{ m}^{-2} \qquad (4)$$

The latent heat flux LE is then derived from equation (3), and its units are Wm^{-2} if L_v has dimensions of joule.kgm^{-1}.

Although the lysimeter cannot normally resolve variations in the evaporation rate over periods of less than one hour, it has nevertheless proved to be a direct and consistently reliable means of measuring LE continuously, with an accuracy of between 10 and 20 per cent; and all the LE data in this paper originates from this source.

The latent heat flux may also be derived, indirectly, from the gradient of specific humidity in the surface layer using the transport equation:

$$LE = -\rho K_q \cdot \frac{dq}{dz} \qquad (5)$$

and measurements of q at six levels are being made for this purpose (see section 6a). Unfortunately, the success of this method depends upon a reliable formulation of the diffusivity coefficient, K_q; and this is normally derived experimentally from the direct measurement of LE and dq/dz over a variety of stability conditions. Recently, a fast response hygrometer ($\sim$ 1 Hz) has been fitted to the Cardington turbulence probe (see section 6b) in order to measure directly the eddy flux of water vapour and, therefore, LE through the equation

$$LE = \rho \overline{w'q'} \qquad (6)$$

The performance of these three methods in deriving LE, ie equations 3, 5, 6, is yet to be evaluated.

6. Measurement of Sensible Heat Flux

The sensible heat flux H cannot be measured as readily as can R_N, G, or LE. Three methods are available for estimating H:

a. aerodynamically, from the gradient of potential temperature using the transport equation

$$H = -\rho C_p K_h \, d\Theta/dz \qquad (7);$$

b. directly, by eddy correlation techniques using the eddy flux equation

$$H = \rho C_p \overline{w' \theta'} \qquad (8);$$

and c. indirectly, using the balance equation (1) itself, in which H is expressed as a residual in terms of R_N, G and LE, thus

$$H = R_N - G - LE \qquad (9)$$

a. Aerodynamic Method

In the transport equation (7), K_h is the eddy diffusivity for heat transfer, and can be described by a generalized relationship of the form

$$K_h = \frac{ku_* z}{\phi_h} \qquad (10),$$

where ϕ_h is the non-dimensional temperature gradient and a function of the stability parameter z/L; see, for instance, Sutton (1953) or Priestley (1959). The representation of ϕ_h is inevitably semi-empirical and many formulations have been published; (see Haugen, 1975). A comprehensive description of ϕ_h, and also ϕ_m, the non-dimensional wind shear, has been given by Businger et al (1971), derived from a data set gathered by AFCRL in Kansas. These functions were found to provide good flux-profile relationships over a variety of

stability regimes, and they have been used in this experiment to derive K_h. They are:

$$\begin{aligned}
&\underline{\text{Unstable}}\ (z/L < -0.1) && \phi_m = (1-15\ z/L)^{-\frac{1}{4}} \\
& && \phi_h = 0.74(1-9\ z/L)^{-\frac{1}{2}} \\
&\underline{\text{Near Neutral}}\ (-0.1 \leqslant z/L \leqslant 0.175) && \phi_m = 1+3\ z/L+10.2(z/L)^2 \\
& && \phi_h = 0.74+3\ z/L+9.2(z/L)^2 \\
&\underline{\text{Stable}}\ (z/L > 0.175) && \phi_m = 1+4.7\ z/L \\
& && \phi_h = 0.74+4.7\ z/L
\end{aligned} \qquad (11)$$

where von Karman's constant was taken to be $k = 0.35$. (Note that many other workers still favour $k = 0.4$).

The stability parameter, z/L, and the Richardson number, Ri, are related by the equation

$$Ri = z/L\ \frac{\phi_h}{\phi_m^2} \qquad (12)$$

However, since it is impossible to solve this equation analytically for negative z/L, z/L is expressed explicitly in terms of Ri by fitting a sixth order polynomial in Ri to a plot of Ri against z/L, and this means that ϕ_m, ϕ_h can then be expressed as functions of Ri. The Richardson number is calculated from 20 minute-meaned profiles of wind speed and potential temperature, to each of which is fitted a log-quadratic regression function of the form $a_o + a_1 \log_e z + a_2(\log_e z)^2$, where z is height and a_o, a_1, a_2 are regression coefficients.

At Cardington, wind speed and temperature are measured at heights of 0.5, 1, 2, 4, 8 and 16 m above the ground using two 20 m high masts. One mast is fitted with a set of six light-weight photo-electric cup anemometers. On the other, dry and wet bulb temperatures are measured using standard platinum-in-

steel resistance thermometers, which are screened from direct radiation by means of weather-proof housings (Fig. 4). A motor is fitted to the mast at each sensing level, and this ensures both elements are ventilated with a steady current of air. A thin paper-tissue wick fitted over each 'wet' element is supplied with distilled water from a bottle, that is mounted on the outside of the housing. The resistance elements on the masts form arms within an extended bridge network, and temperature changes at each level are translated into voltage differences, which are logged in the recording laboratory. Temperature differences between one level and another on the mast cannot be measured with an accuracy much better than $0.1^{\circ}C$. Both temperature and wind speed are sampled at two-minute intervals, the wind measurements representing the mean speed during the preceding two-minute period, and data sets each of several days duration can be gathered. The masts can be lowered for servicing and routine maintenance; eg calibration, replacement of wicks and topping up of water bottles.

The friction velocity u_* in equation (10) is calculated from the relationship

$$u_* = \frac{k(z-d)}{\phi_m} \frac{du}{dz} \qquad (13)$$

where d is the zero-plane displacement. Since the grass over the experimental site is cut regularly, $d \ll z$ and has therefore been ignored. By substituting values of ϕ_h and $_*$ into equation (10), K_h and, hence, H can be calculated.

It should be noted that the statistics upon which equations (11) are based are valid only for $Ri < 0.21$ or so, and this

restricts their application in very stable conditions. However, in these circumstances turbulence in the surface layer is probably so small that the (downward) sensible heat flux is virtually zero anyhow.

The accuracy with which H can be calculated by this aerodynamic method is clearly limited by the semi-empirical description of ϕ_h. At Cardington, it is also limited by the restricted fetch over grass, and therefore by the relatively shallow constant flux layer (4-8 metres deep) at the site; (see Wood, 1977). For these reasons, the sensible heat flux cannot normally be measured by this method to much better than 20 per cent.

b. Eddy Correlation Method

The eddy correlation method is essentially the only way of measuring H directly, and the fast response instrumentation afforded by the Cardington turbulence probe is used for this purpose; see, for example Readings and Butler (1972), and Caughey (1977). The sensors on the probe measure the instantaneous components U, V, W of the wind vector and the temperature T, and, more recently the specific humidity q. The eddy heat flux, defined by equation (8), is derived from the fluctuating quantities w' and T' through statistical correlation theory, and it can be measured to within 10 per cent. The probe is mounted on an extensible, mobile mast which is raised to a height of 16 m, and the output signals are sampled at a frequency of several hertz. The large physical volume of data generated tends to limit the length of each data set to two or three hours duration, in contrast to several days' worth of heat flux data which is available from wind and temperature profile data.

For these reasons, long term (eg daily) measurements of H are based upon the aerodynamic method, profile data permitting, and eddy flux measurements with the probe are used periodically to check the performance of this method. A preliminary comparison of both methods (a) and (b) is shown in Fig. 5, using data gathered in 1976. Although there is scatter about the 45° axis, this graph does show modest agreement between the aerodynamic and eddy correlation methods, with a standard error of probably around 30 Wm^{-2}.

c. Residual Method

The validity of estimating H as a residual quantity using equation (9) depends, of course, upon the energy balance equation (1) being satisfied in the first place. In practice this equation is not satisfied because the measurement of R_N, G, LE and H is far from precise. The resulting "imbalance" is given by $R_N - (G + LE + H)$. Measurements of these energy balance components over a wide variety of conditions during 1976 show that this imbalance is a rather unpredictable quantity, but on the whole equation (1) is found to be satisfied within the error limits associated with the components. This method has therefore been used to derive H in the absence of profile measurements, with a standard error of between 20 and 40 Wm^{-2}.

PRESENTATION OF DATA

7. Some Typical Soil Heat Flux Profiles

Before presenting some typical measurements of the soil heat flux it will be useful to review briefly the relationships governing the flow of heat in the ground. All natural ground consists essentially of (a) soil, (b) free water, and (c) air, occupying the spaces

between the soil particles. The relative proportion of these components governs the specific heat per unit volume (ρC) of the soil at any depth, z. It is only a constant for perfectly dry soil, and increases in value with the water content of the soil; see, for example, Geiger (1950).

The rate of flow of heat through the soil G is given by the conductivity equation

$$G = - k_s \partial\theta/\partial z \qquad (14)$$

where k_s is the thermal conductivity, and $\partial\theta/\partial z$ the vertical temperature gradient in the soil. k_s varies in the same sense as the density and soil water content, just like the specific heat (ρC).

The rate of change of temperature is related to the heat flux divergence in the soil through the equation

$$\frac{\partial\theta}{\partial t} = - \frac{1}{(\rho C)} \frac{\partial G}{\partial z} \qquad (15)$$

By eliminating G from equations (14) and (15), the heat conduction equation in one dimension is obtained, assuming k_s is constant with depth, thus:

$$\frac{\partial\theta}{\partial t} = K \frac{\partial^2\theta}{\partial z^2} \qquad (16)$$

where $K = k_s/\rho C$ is the thermal diffusivity of the soil (units: $M^2 sec^{-1}$). The solution to this equation depends upon the boundary conditions imposed, but if a sinusoidal time-dependent boundary condition, of angular frequency ω, is applied at the surface ($z = 0$) in order to simulate the daily radiation wave at the surface, a solution can be derived for the soil heat flux G at any depth z, thus:

$$G(z,t) = G_0 e^{-\lambda z} \sin(\omega t - \lambda z) \qquad (17)$$

where $\lambda = \sqrt{\frac{\omega}{2K}}$

This describes a progressive wave of phase velocity V, given by

$$V = \sqrt{2K\omega} \qquad (18)$$

whose amplitude decays exponentially from its surface value Go, and lags in phase linearly with depth. The amplitude, A_z, of the soil heat wave at any depth z is related to the amplitude, A_{ref}, at some given reference depth Z_{ref} thus:

$$A_z / A_{ref} = \exp[\lambda(z_{ref} - z)] \qquad (19)$$

(The solution of equation (16) for the temperature $\Theta(z,t)$ has a similar form as equation (17), but it lags in phase by $\pi/4$ relative to G (z, t)). Equation (19) can be used to determine the "penetration depth" of either the daily or annual heat wave into the soil. This depth is the level at which the amplitude of the soil heat wave is reduced to one per cent of its surface value.

Fig. 6shows profiles of soil heat flux on June 26 1976, during a hot, fine period at Cardington, at various depths between 5 and 80 cm. The net radiation at the surface is included for comparison, and this curve reaches its maximum daytime value at around 1200 GMT. The associated heat wave generated at the surface is conducted down into the ground with an increasing time (phase) lag, as predicted by equation (17). The wave travels with a mean velocity of 3.5 cm hr^{-1}, and it reaches the 40 cm level in late evening. Since ω can be obtained from the half-period of the wave motion, which is about 10 hours, equation (18) can be used to derive the value K = 0.54 x 10^{-6} $M^2 sec^{-1}$ for the mean diffusivity in the top 40 cm layer of soil. A value of 51 cm for the penetration depth of the diurnal soil heat wave is then obtained from equation (19). This value agrees well

with the experimental data in Fig. 6, since the diurnal oscillation in the soil heat flux profile disappears between 40 and 80 cm. The steady downward flux of 5 Wm^{-2} at 80 cm reflects the longer term (ie seasonal) warming of the soil at this depth.

It is interesting to examine how the observed amplitude reduction with depth shown in Fig. 6 compares with theory, as given by the ratio Az/A_{ref} in equation (19). This ratio has been tabulated in column 2 of Table 1, expressed in terms of the peak-to-peak amplitude (ie diurnal range), A_5, of the heat wave at 5 cm. Column 3 gives the diurnal range of the soil heat flux measured at each depth z, (though the surface value of 145 Wm^{-2} is based on the method of extrapolation mentioned earlier). If the observed diurnal range at 5 cm is multiplied by the percentages of column 2, the theoretical variation with depth of the peak-to-peak amplitude is obtained, and this is shown in column 4. A comparison of columns 3 and 4 indicates that the observed amplitude decay agrees well with the exponential law of equation (19), except at the surface where the theoretical and extrapolated values differ noticeably. The agreement is not perfect because various assumptions are implicit in equation (19). Firstly, soil is not a homogeneous medium. Density, conductivity, and specific heat can all vary with depth, in which case K is no longer a constant. To illustrate this point, it can be seen in Fig. 6 that the mean phase velocity of the soil heat wave in the 20-40 cm layer, (which depends on K through equation 18)), is half that in the 10-20 cm layer. Secondly, the nature of the driving wave at the surface $z = 0$ is only approximately sinusoidal in clear weather. The shape of the diurnal radiation R_N wave is perhaps better described by a normal (ie "Gaussian") function. In cloudy weather, R_N would

be such a complex function of time that the solution of equation (16) would be impossible.

In order to illustrate the considerable heat flux divergence that typically occurs within the top layer of soil during a fine period, Fig. 7 shows isopleths of heat flux on a depth-time plot over a three day period toward the end of June 1976. The gradient of the two sloping lines on this diagram gives the mean downward velocity of the heat wave into the ground. The diagram demonstrates how difficult it can be to obtain a realistic measure of the surface soilheat flux in these conditions.

8. Typical Diurnal Variation of Surface Layer Temperature and Wind Shear on a Fine Day

In Fig. 8 the evolution of the surface layer temperature profile is shown for a fine day during August 1976, with meaned hourly profiles (GMT) plotted against a log-height scale. The diagram shows that the overnight inversion in the surface layer breaks down shortly after sunrise (0500 GMT), with a near neutral layer establishing itself for an hour or two, during which time the temperature rises rapidly. During the morning the static instability of the layer increases steadily, and a temperature lapse of between 2° and 2.5°C develops between the 0.5 and 16 m levels. This superadiabatic gradient does not change significantly during the midday period, ie 1000-1400 GMT. From mid-afternoon onwards, however, the layer begins to cool from the surface, and it becomes neutrally stable at around 1700 GMT, about an hour before sunset. During the evening an inversion develops and strengthens in the layer, and is accompanied by a steady fall in temperature. This cooling, however, is considerably less rapid than the warming which occurs after dawn.

Fig. 9 shows the wind shear in the layer during the same day, when a moderate southeasterly airstream covered the area. It illustrates the classical departure of the vertical wind profile from the log law in non-adiabatic conditions. When the layer is stable, eg around dawn and during the evening, the profile is curved toward the U axis because $^{du}/d(\log z)$ increases with height. However, as the superadiabatic temperature gradient develops the curvature reverses its sense very noticeably. This behaviour is, of course, described by the well-known differential relationship, $^{du}/d(\log_e z) = \left(u_*/k\right)\phi_m$, where the dependence of ϕ_m on stability is given in equations (11). It may also be noted that the wind speed in the lower part of the surface layer is closely associated with the change in static stability; it increases rapidly during the morning, changes little during the forenoon and afternoon, and decreases slowly in the evening.

9. Discussion of the Surface Energy Budget: April-August 1976

The summer of 1976 was exceptionally dry in Britain, and many accounts have been written about th is period of drought; see, for instance, Perry (1976), Green (1977), and Ratcliffe (1977). In order to illustrate the effect which this drought had on evaporation at Cardington, Fig. 10 gives a comparison of the evaporation from open water and the evapotranspiration from grass with the average for the previous six years. It will be noted that, although evaporation increased rapidly during the spring and early summer to reach a maximum of 156 mm in July, evapotranspiration during the same period actually fell, reaching a minimum of less than 40 per cent of the mean by August. This reduced evapotranspiration exerted a most noticeable effect on the surface energy budget during this period.

Figs. 11(a), (b) show the daily variation of the components in the energy budget at Cardington, averaged over the period 0600 to 1800 GMT, and also the daily rainfall, from April to August 1976. Of the four terms in the budget it will be noted that the net radiation R_N is generally the largest, and, furthermore, is usually subject to the greatest daily changes. This is because R_N is strongly dependent on the elevation of the midday sun, and on meteorological factors such as cloud cover and depth, and atmospheric turbidity. The other components in the energy budget reflect the variations in R_N to a greater or lesser degree. Soil heat flux, G, for instance, follows R_N closely, but with greatly reduced amplitude. In fact, any one of the four components in the balance equation can fluctuate rapidly, and the nature of the energy budget can therefore change significantly daily; see for instance, the periods 24-26 May, 18-22 June, and 14-18 July.

The latent heat flux LE is a generally complex function of the net radiation R_N, the drying power of the wind, and the moisture content of the soil. Where there is an adequate supply of soil moisture, LE is a strong function of R_N. During April and May this was the case, and LE was typically the second larget term in the energy budget, exceeding H and G (Fig. 11(a)). However, as the summer advanced and the ground water supply was depleted through evaporation and transpiration, LE fell steadily and became the smallest term in the budget during August, accounting for less than 10 per cent of R_N (Fig. 11(b)). During the same period the sensible heat flux, H, increased in magnitude and became the second largest term. When it did rain LE recovered somewhat, usually at the expense of H; see, for instance, the 15-22 July. However, this

modification to the energy budget was typically shortlived, and the newly acquired ground water was soon depleted through evaporation. A large reserve of soil moisture, regularly replenished by rainfall, is necessary to support evapotranspiration near the potential rate during the summer.

A detailed hourly analysis of the energy budget on six days, including cloud cover and screen temperature, is given in Figs. 12(a)-(f), and it illustrates some aspects of the diurnal variation of the energy budget during the spring and summer of 1976. On fine days, R_N reaches a midday maximum of between 400 and 500 Wm^{-2}; see Figs. 12(b, c, e, f). The soil heat flux G tends to lag in phase behind R_N by an hour or so, as is illustrated for the partly cloudy days shown in Fig. 12 (a, d). This phase lag implies that G is not a true surface value and probably reflects a limitation of the extrapolation method discussed in section 4. The sequence of diagrams in Figs 12 illustrates well the role reversal of LE and H during the summer. The period from 23 June to 7 July was particularly hot, during which daytime temperatures exceeded 30°C, and the latent heat flux fell rapidly; compare Fig. 12(d) with 12(e). From 20 July to 27 August virtually no rain fell at Cardington, and the sensible heat component dominated the daytime energy budget. It is worthwhile noting how the small LE term became less and less dependent on R_N, responding mainly to any available surface moisture. For example, overnight dewfall on clear days tended to boost LE for several hours after dawn during this period. Indeed, the daytime maximum of LE was sometimes reached very early in the day during August, and this contrasts with the obvious R_N dependence earlier in the year, eg 6 April (Fig. 12a).

Despite the apparent absence of surface moisture by day in August, (the ground was cracked and backed hard), the grass cover on the lysimeter continued to transpire some water, although it amounted only to around 0.4 mm per day. Because the grass on the lysimeter did seem marginally greener than the surrounding surface, it may have overestimated the latent heat flux at this time. (Evaporation from non-irrigated lysimeters is sometimes criticized for being unrealistically small during periods of drought).

Although the soil and sensible heat fluxes are primarily functions of the net radiation R_N, a large latent heat flux can reduce the size of G and H appreciably, particularly if R_N is not very big. In some cases, the chilling effect at the surface due to strong evaporation can even drive these terms negative. Fig.12(d) gives an example of a day, 20 June, on which the energy balance was dominated by a large LE term following some rain during the previous 24 hours. During the morning the latent heat flux increases so rapidly in response to a drying wind that G and H are suppressed for much of the morning. H is even driven negative for a short time around 0900 GMT. The maximum sensible heat flux on this day is delayed till late afternoon, after the latent heat term has long passed its peak. It is noteworthy that the rise in air temperature during the day was very much smaller than, say, that on 24 May (Fig. 12c), when H was much greater.

10. Concluding Remarks

From the measurements of the energy budget during the spring and summer of 1976, the following summary can be made.

i. Individual terms in the energy budget can be subject to rapid short term (eg hourly) fluctuations. The budget,

itself, can alter significantly from one day to the next.

ii. Of the four components, the net radiation, R_N, is generally the largest by day, and changes in R_N are reflected in the other three components to a varying degree.

iii. The latent heat flux, LE, is primarily dependent on R_N, provided there is an adequate supply of moisture in the ground to permit transpiration at approximately the potential rate. When, however, the reservoir of water in the soil becomes seriously depleted as, for instance, during a drought, then LE depends less on R_N and rather more on available surface moisture, (eg dewfall).

iv. When an appreciable fall of rain does occur during an otherwise dry period, the latent heat flux can recover rapidly to a value near the equivalent potential rate of evaporation. This is usually a temporary feature of the energy budget, unless there is renewed rainfall.

v. The soil and sensible heat fluxes are functions of R_N by day. The soil heat flux usually constitutes between 15 and 25 per cent of R_N, but the sensible heat flux is very dependent upon the magnitude of LE.

vi. The incident radiation is conducted down through the soil as a heat wave, with an amplitude that decreases exponentially, and a phase lag that increases linearly, with depth. The diurnal wave does not penetrate much deeper than 50 cm (in clay soil).

The exceptional character of the summer of 1976 has served well to illustrate how quickly the surface energy budget can change over various time scales, and it has demonstrated how much the components in the budget depend upon one another.

List of References

Blackwell, M J 1963 "The role of evaporation in the surface energy balance"; The Water Relations of Plants. Blackwell Scientific Publications.

Businger, J A, Wyngaard, S C Izumi, Y and Bradley, E F 1971 "Flux-Profile relationships in the atmospheric surface layer"; J. Atmos. Sci., 28 p 181-189.

Caughey, S J 1977 "The Cardington turbulence instrumentation"; unpublished Met O Turbulence and Diffusion Note No 82.

Geiger, R 1950 "The climate near the ground"; Harvard University Press, Cambridge, Mass. (revised edition 1965).

Green, J S A 1977 "The weather during July 1976 - some dynamical considerations of the drought"; WEATHER 32 No 4, Royal Met. Society.

Haugen, D A 1973 "Workshop on micrometeorology" Ed Duane A Haugen, American Met Society, Boston.

Munn, R E 1966 "Descriptive micrometeorology"; Academic Press, New York.

Penman, H L 1949 "The dependence of transpiration on weather and soil conditions". J. Soil Science 1 1949.

Penman, H L	1956	"Evaporation - an introductory survey". (Proceedings of meeting on physics in agriculture, Wageningen, Netherlands. 7-13 Sept 1955). Netherlands Journal of Agricultural Science.
Perry, A H	1976	"The long drought of 1975/76"; WEATHER, 31, No 10, Royal Met. Society.
Priestley, C H B	1959	"Turbulent transfer in the lower atmosphere"; University of Chicago Press, p. 19-38.
Ratcliffe, R A S	1977	"A synoptic climatologist's viewpoint of the 1975/76 drought"; Met. Mag. 106, p 145-154.
Readings, C J and Butler, H E	1972	"The measurement of atmospheric turbulence from a captive balloon"; Met. Mag. 101, 286-298.
Smith, F B and Carson D J	1974	"Some thoughts on the specification of the boundary layer relevant to numerical modelling"; unpublished Met O Turbulence and Diffusion Note No 58.

Smith, F B 1975 "Brief notes on the specification of the boundary layer in terms of external readily assessed parameters. Unpublished Met O Turbulence and Diffusion Note No 63.

Sutton, O G 1953 "Micrometeorology"; p 238. McGraw Hill Book Co Inc.

Wood, N L H 1977 "A field study on the representativeness of turbulent fluxes of heat and water vapour at various sites in southern England". Q. J. Royal Met. Society 103, p 617-624.

LIST OF FIGURES

Figs 12 : Hourly Energy Budget, Cloud cover and Screen Temperature at Cardington:

(a) 6 April 1976 (c) 24 May 1976 (e) 1 July 1976

(b) 7 May 1976 (d) 20 June 1976 (f) 16 August 1976

x - - - x Net Radiation, R_N

x ——— x Soil Heat Flux, G

• ..... • Latent Heat Flux, LE

⊙ ——— ⊙ Sensible Heat Flux, H

+ ——— + Screen Temperature, T °C

Cloud cover is indicated by the row of plotting symbols at top of each diagram. Abbreviations beneath give cloud type. Significant weather is given by the symbols of the "Present Weather" (ww) synoptic code.

TABLE 1 Comparison of the Actual Soil Heat Flux Profile with the Theoretical Prediction.

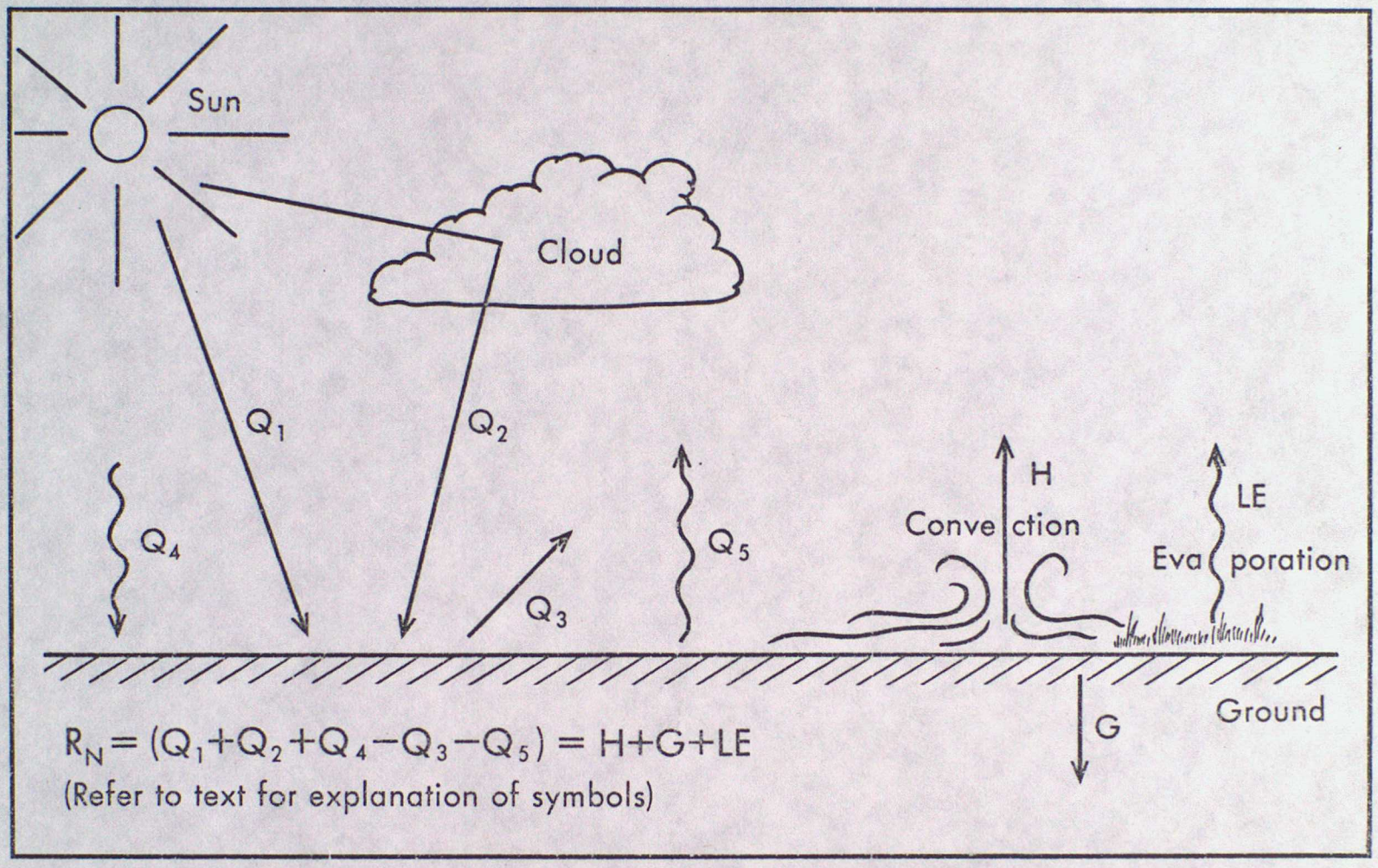

Fig. 1. The principal components of the energy balance over a horizontal surface.

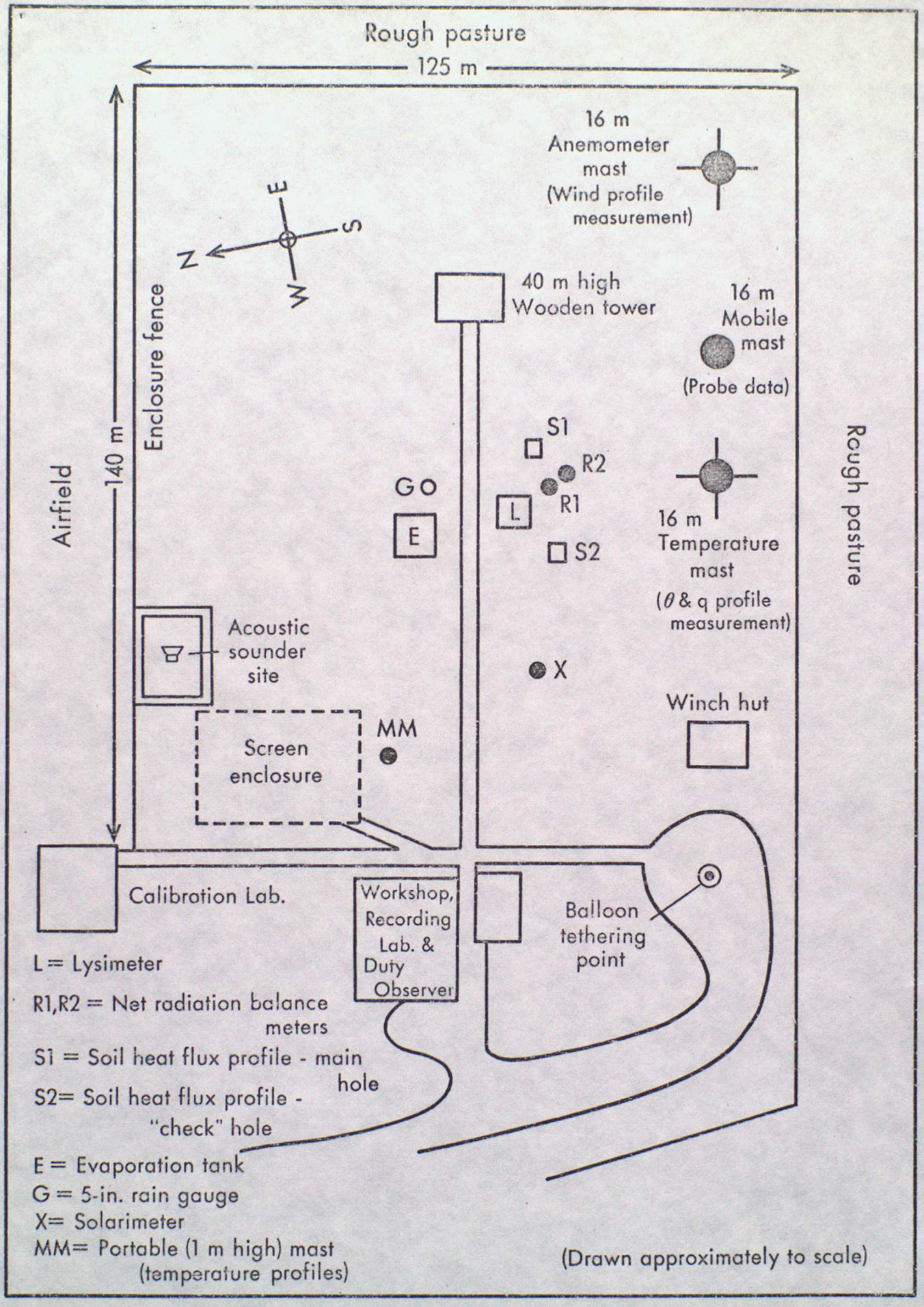

Fig. 2. Plan view of the instrument enclosure at MRU Cardington.

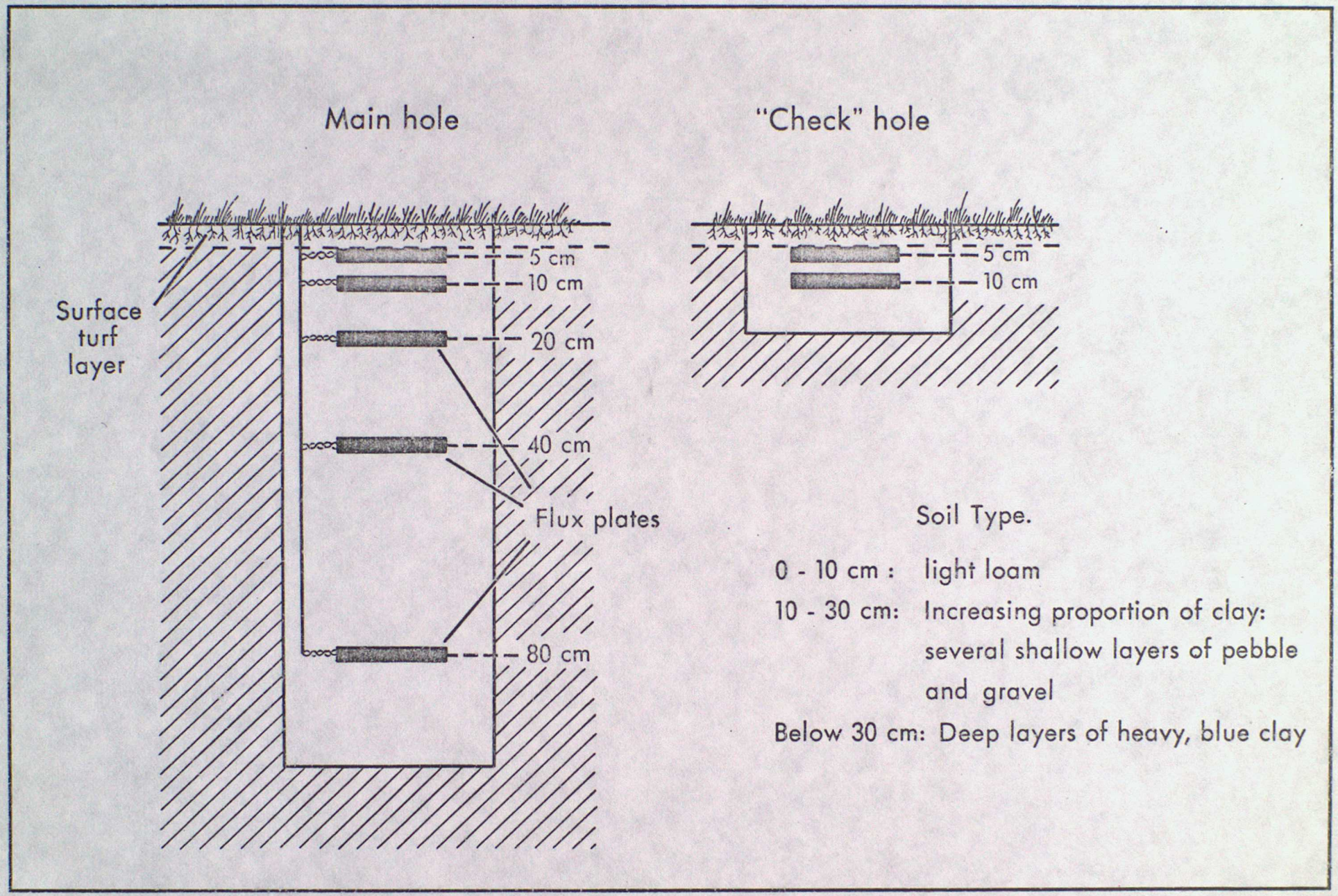

Fig. 3. Measurement of Soil Heat Flux.

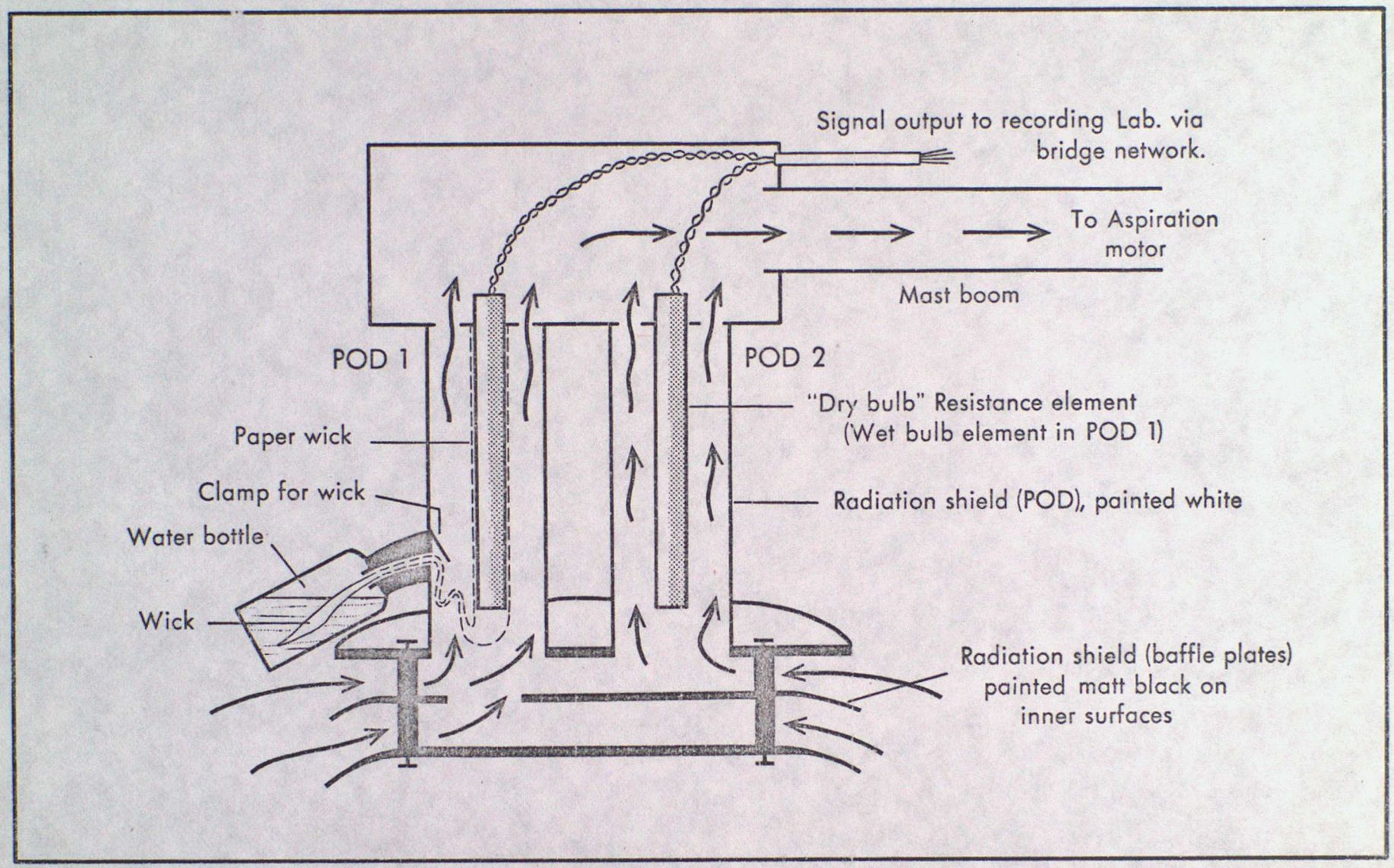

Fig. 4. Measurement of Dry bulb and Wet bulb temperature profiles — cross-section through the radiation screen.

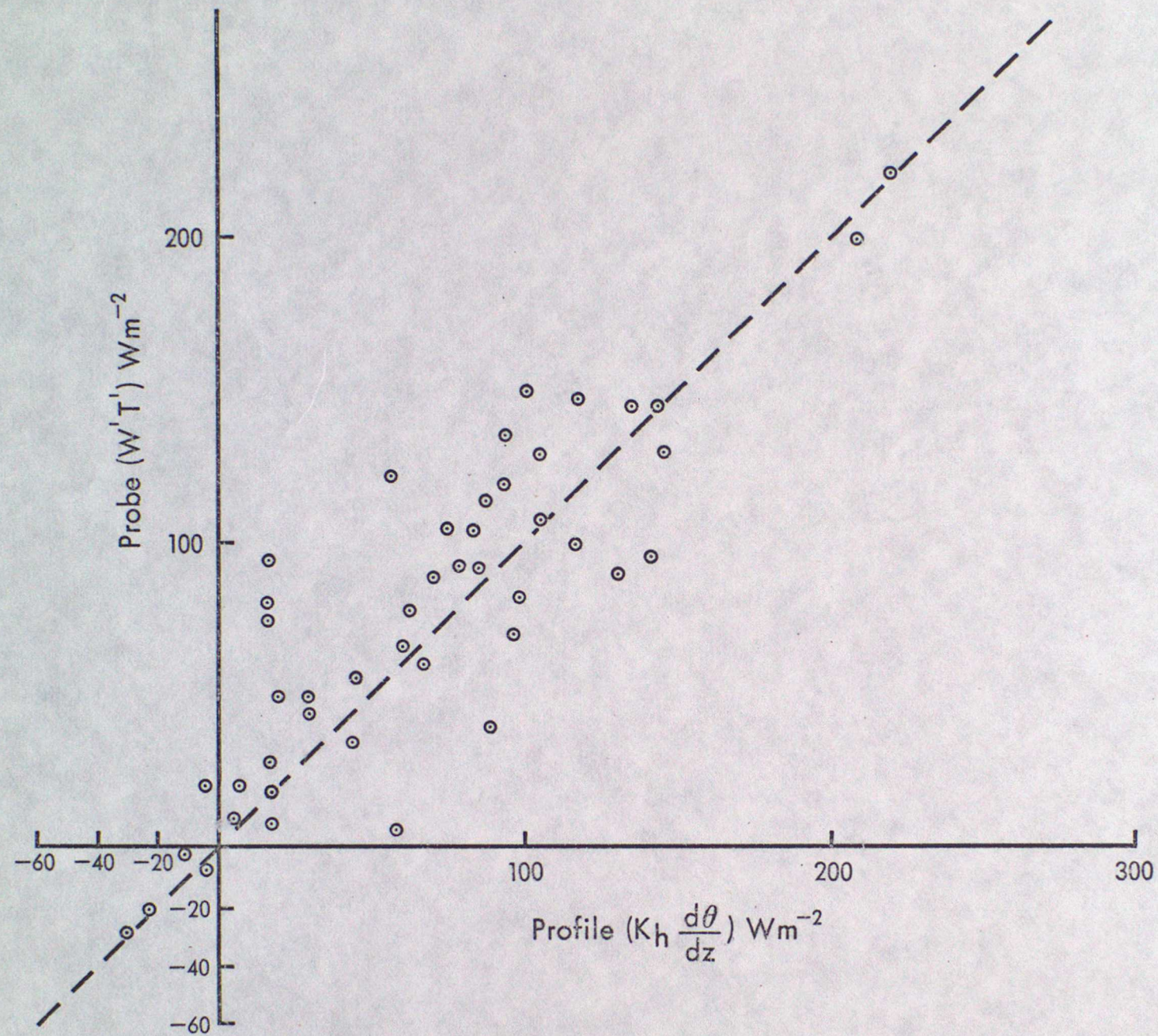

Fig. 5. Comparison of Probe and Profile-derived sensible heat flux measurements - 1976

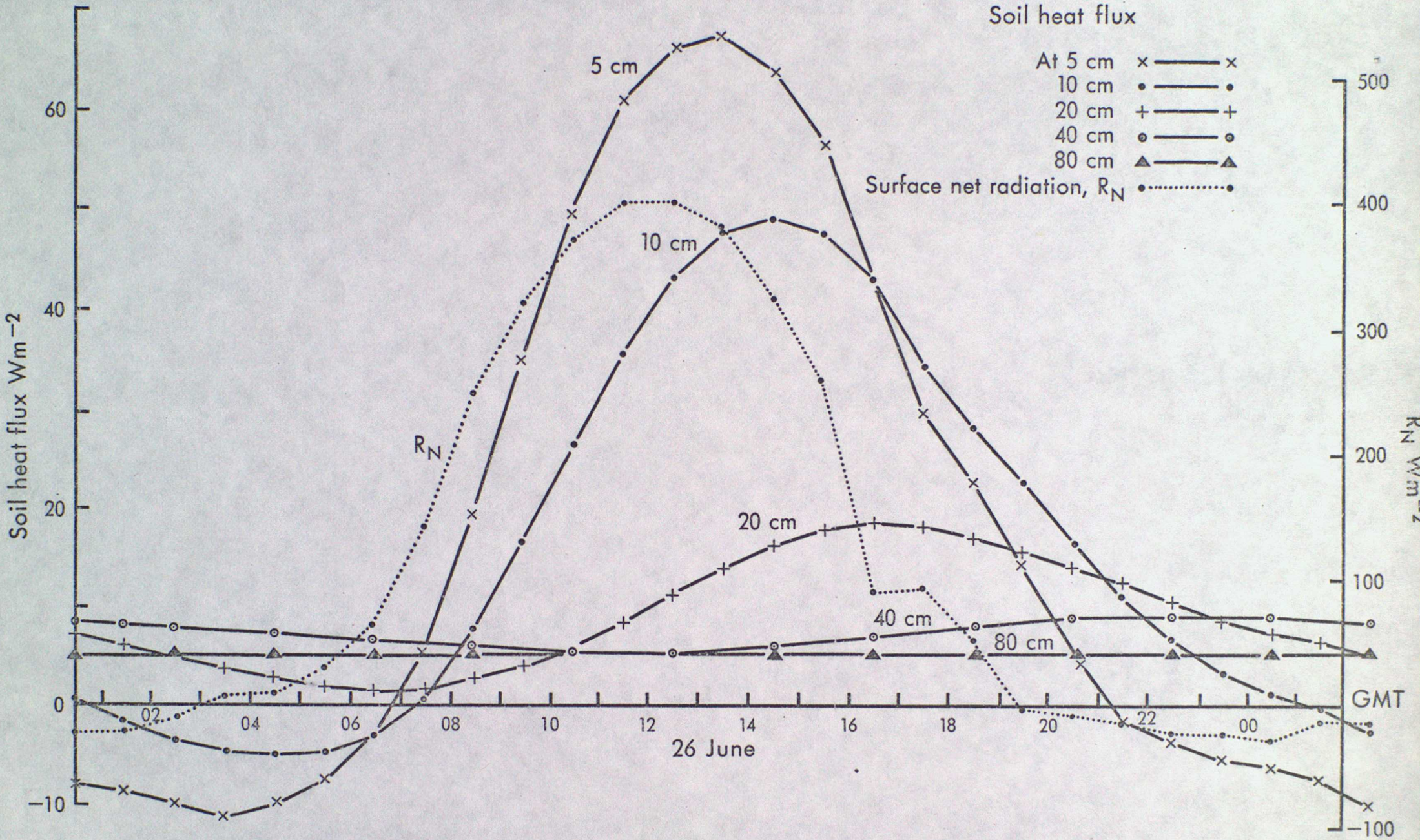

Fig. 6. Variation of Soil heat flux with depth at Cardington - 26 June 1976

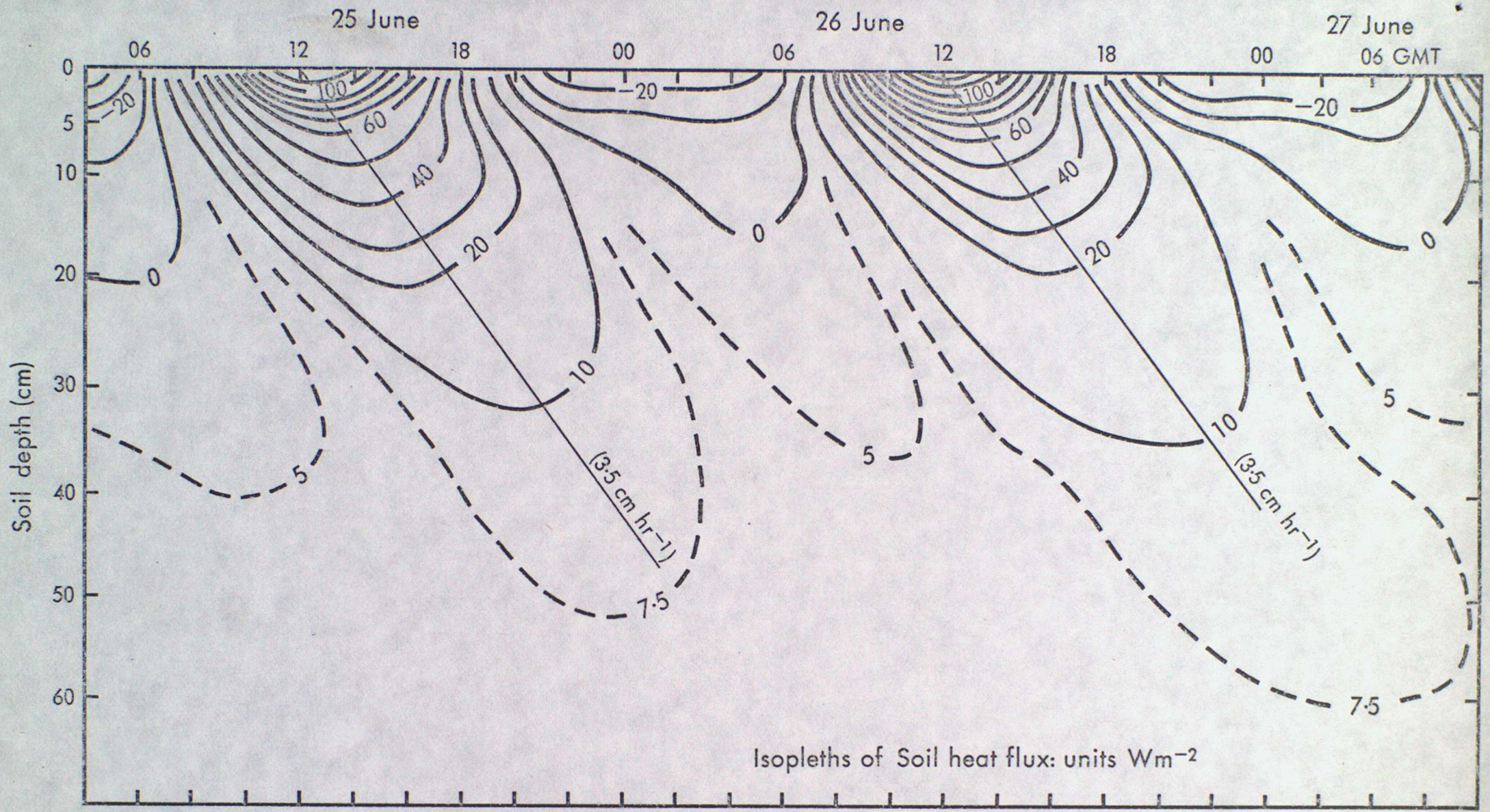

Fig. 7. The diurnal variation of Soil heat flux at Cardington: 25-27 June 1976

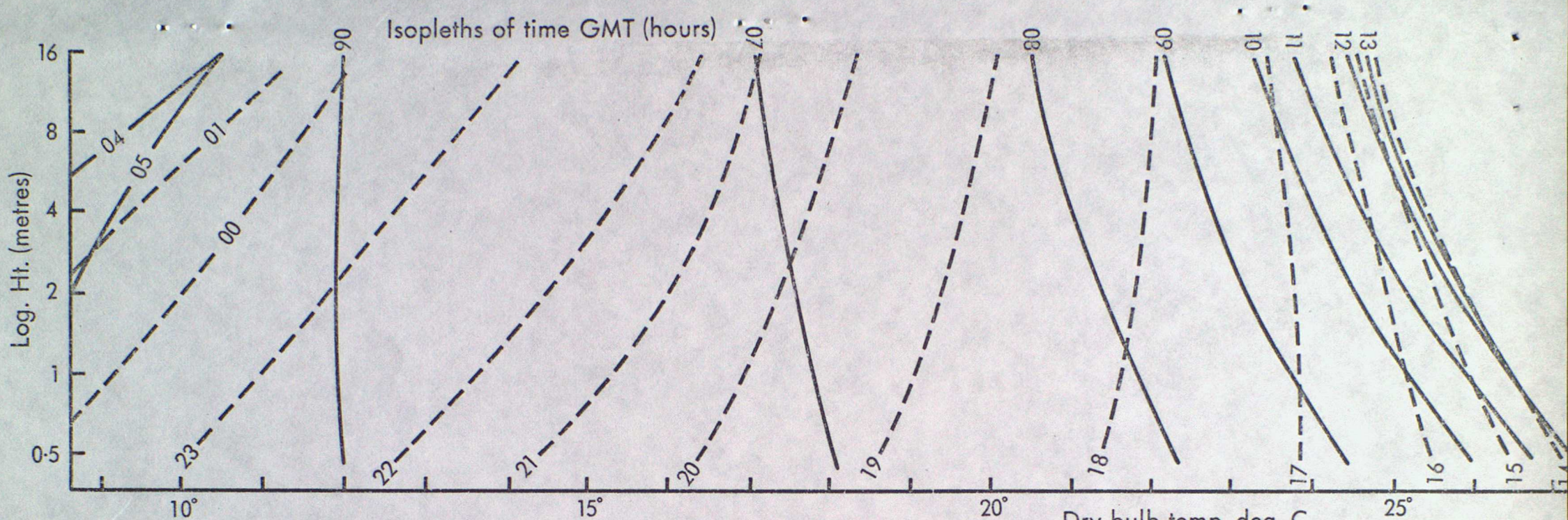

Fig. 8. Temperature structure in the surface layer on 23 August 1976

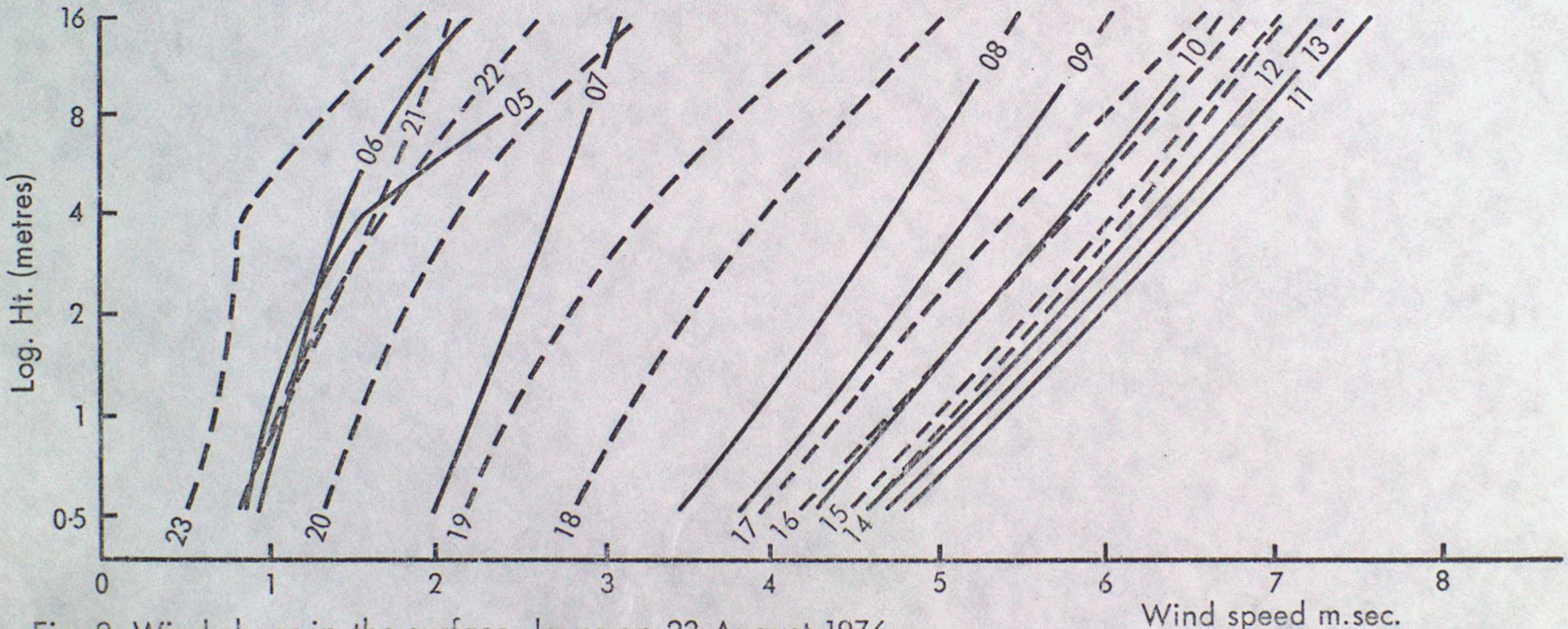

Fig. 9. Wind shear in the surface layer on 23 August 1976

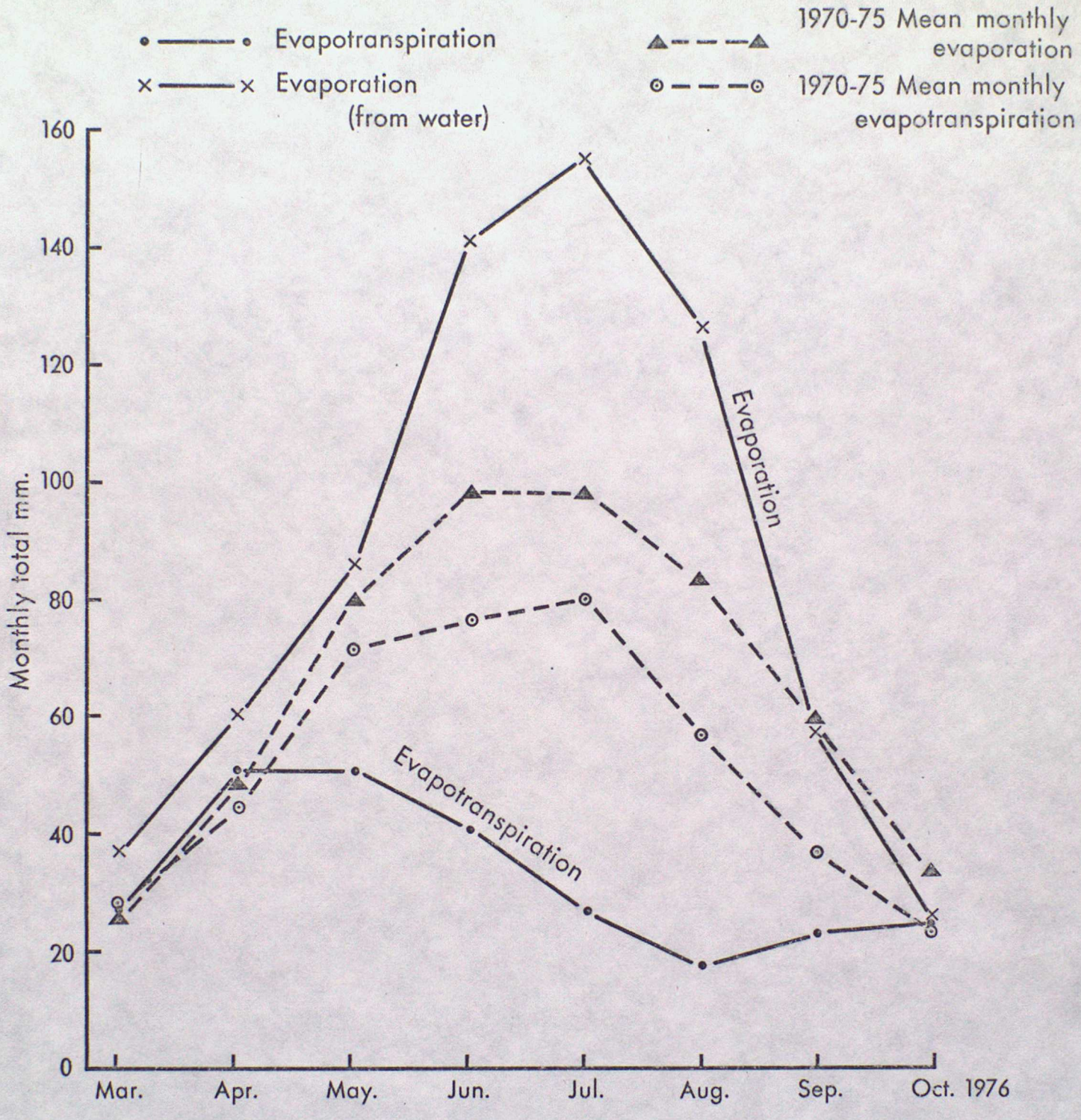

Fig. 10. Monthly evaporation at Cardington – March to October 1976

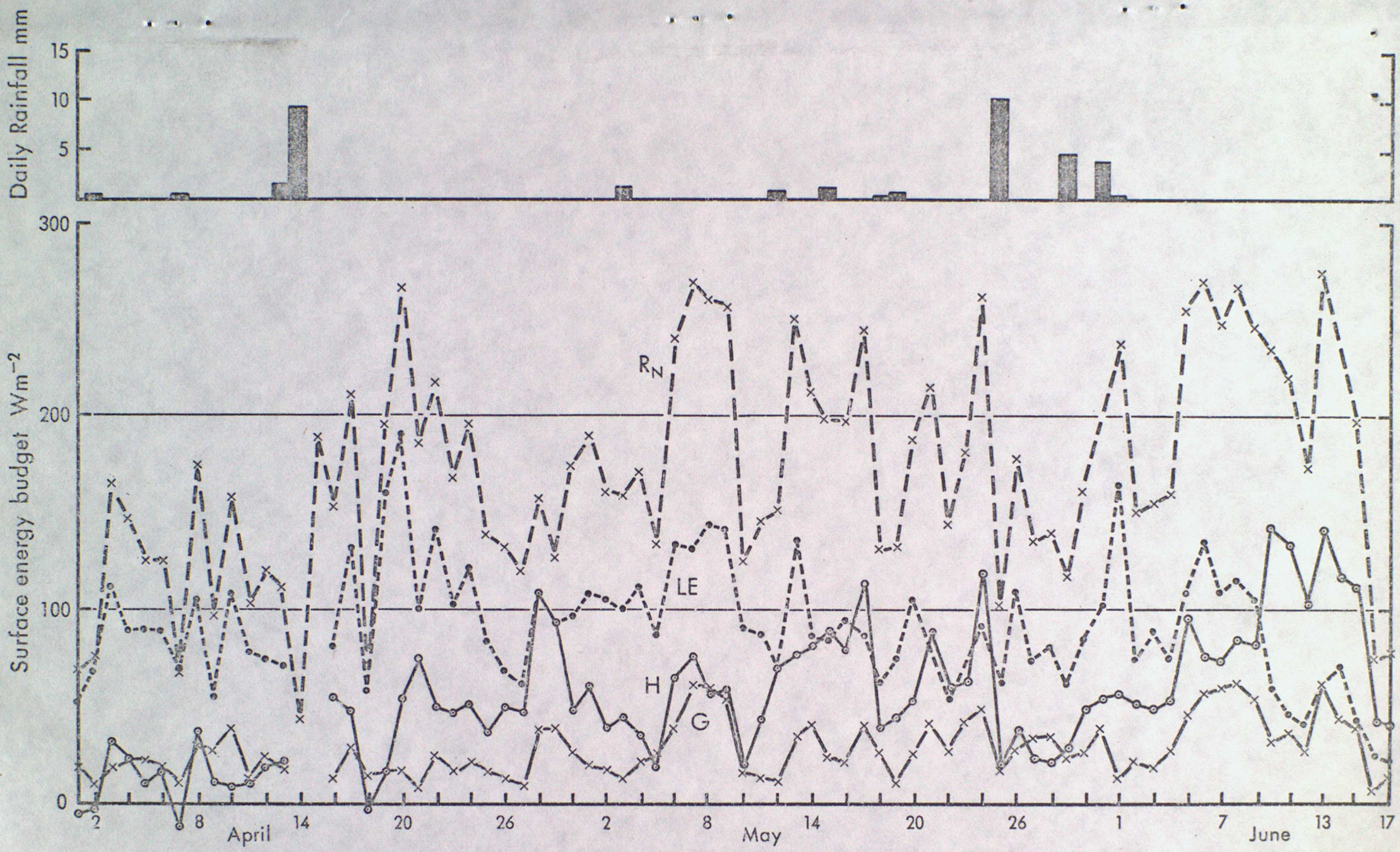

Fig. 11 (a) Mean daily (0600 - 1800 GMT) Surface energy budget at Cardington: April to June 1976

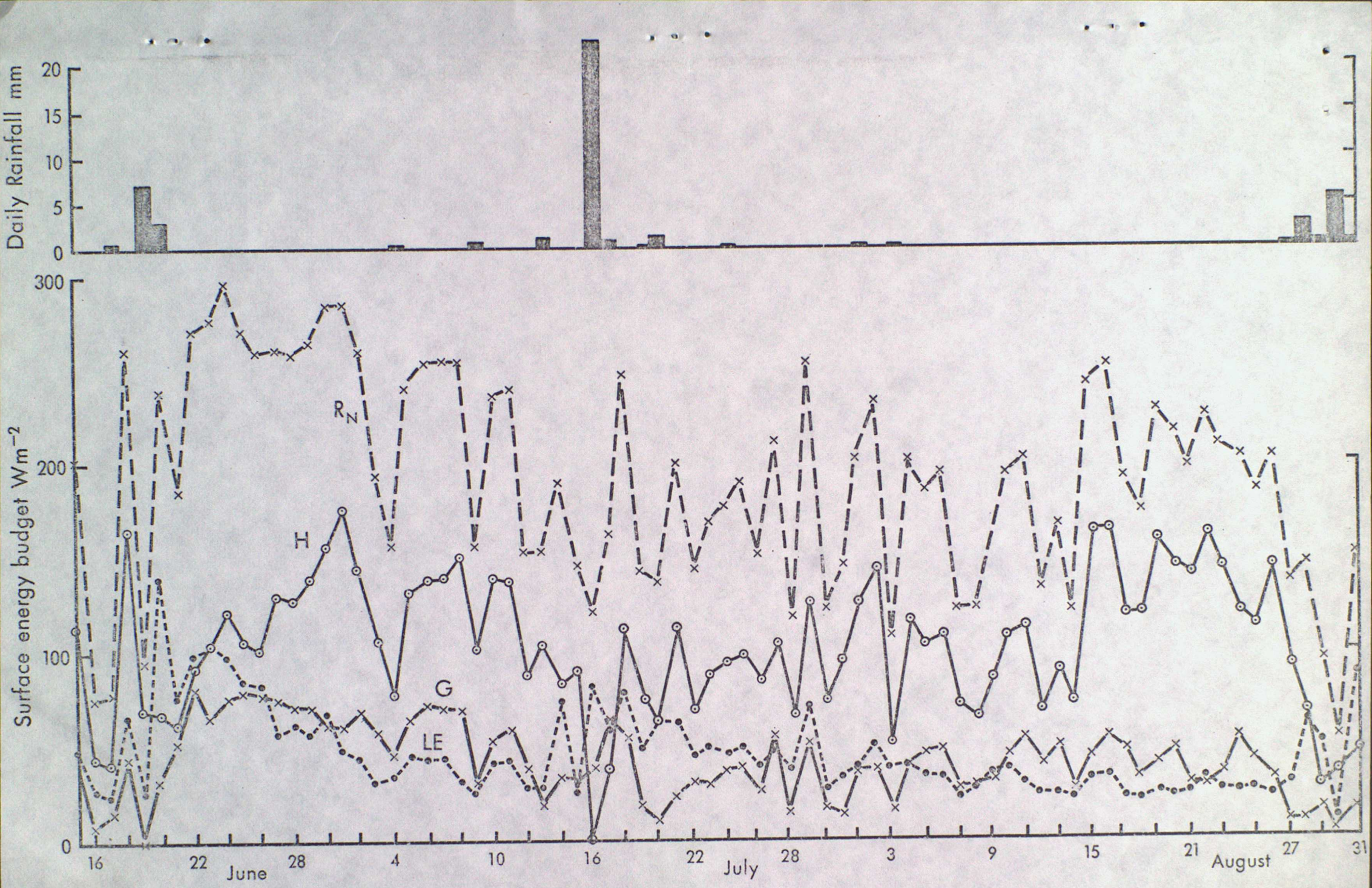

Fig. 11 (b) Mean daily surface energy budget at Cardington: (0600 - 1800 GMT) June to August 1976

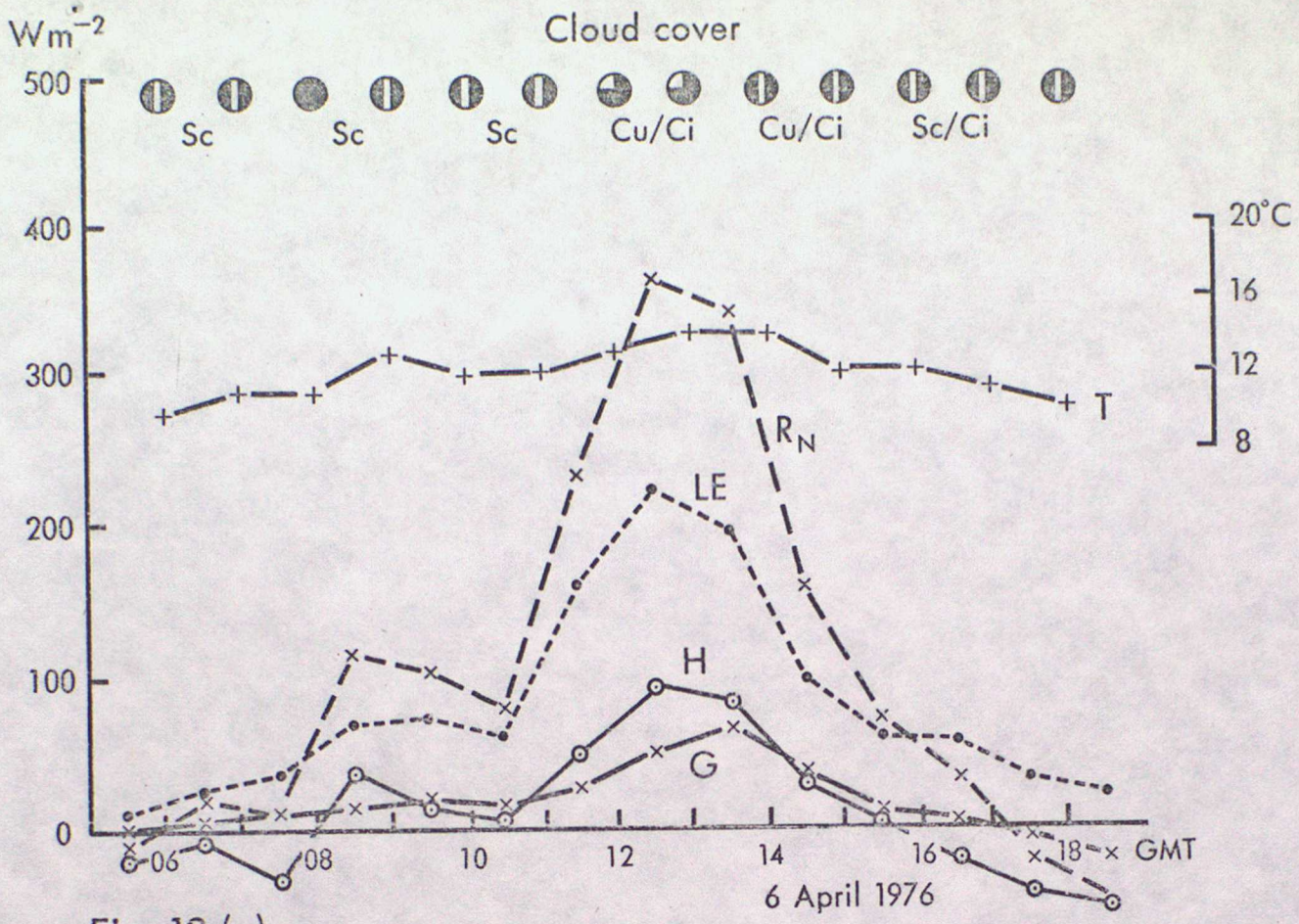

Fig. 12 (a)

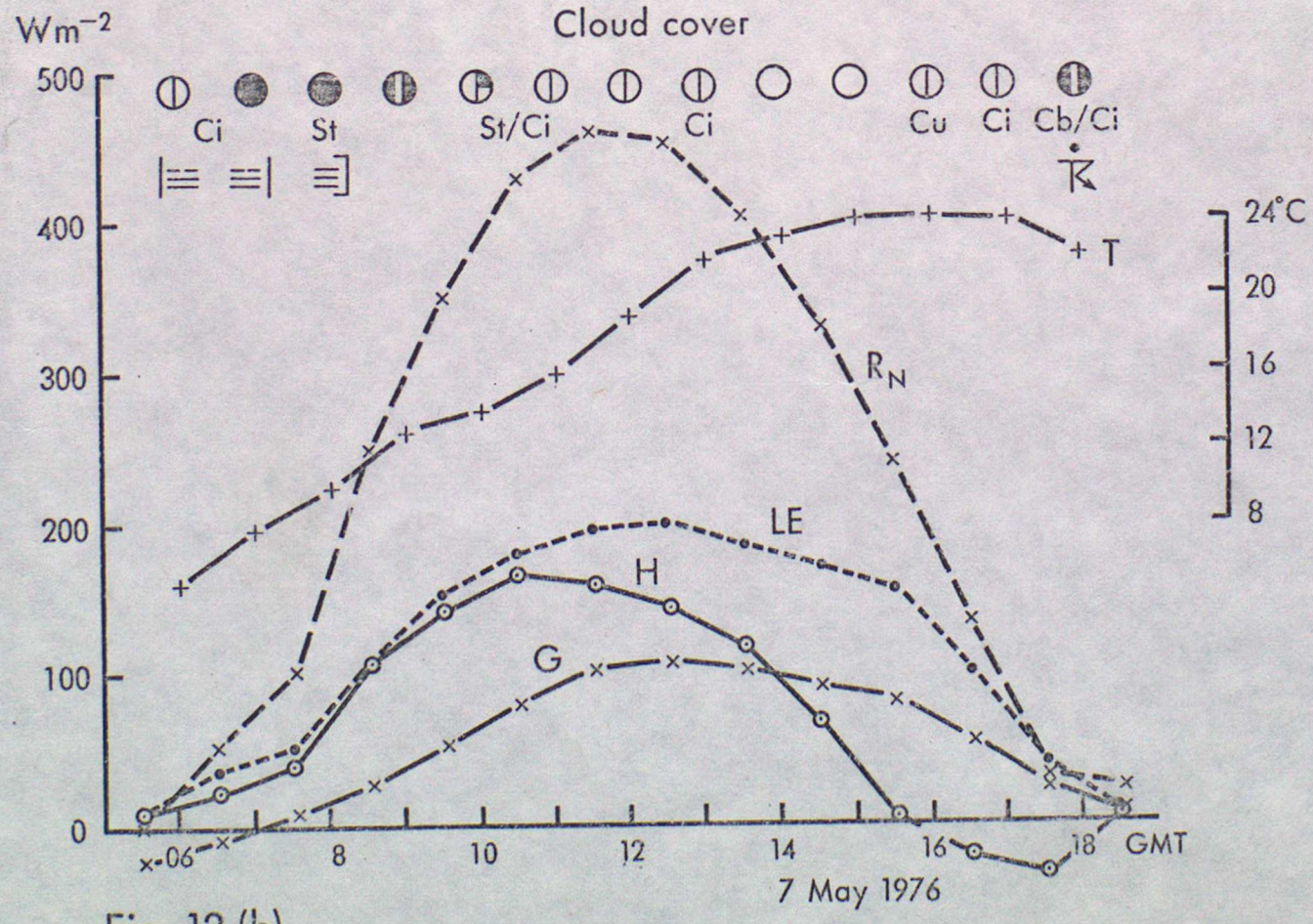

Fig. 12 (b)

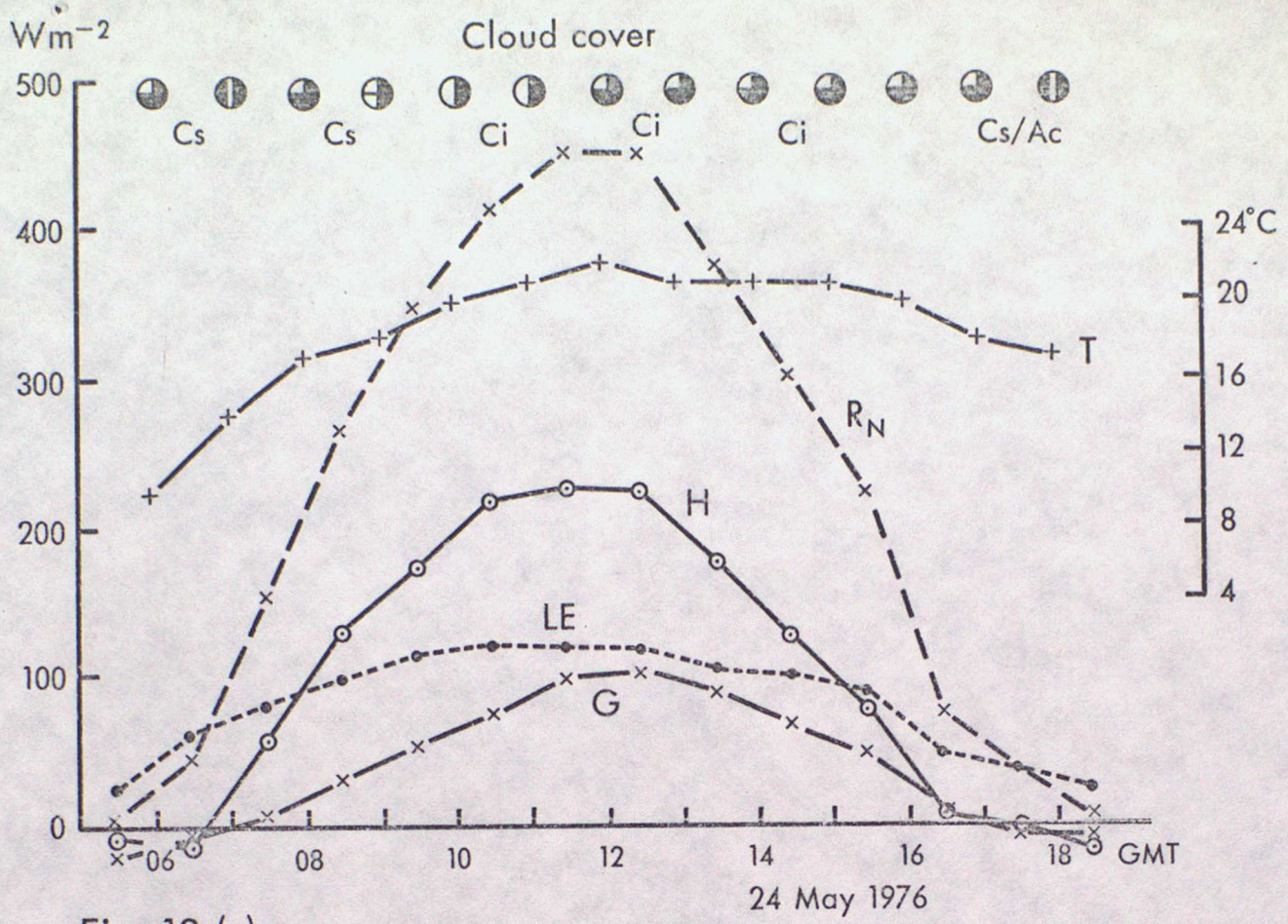

Fig. 12 (c)

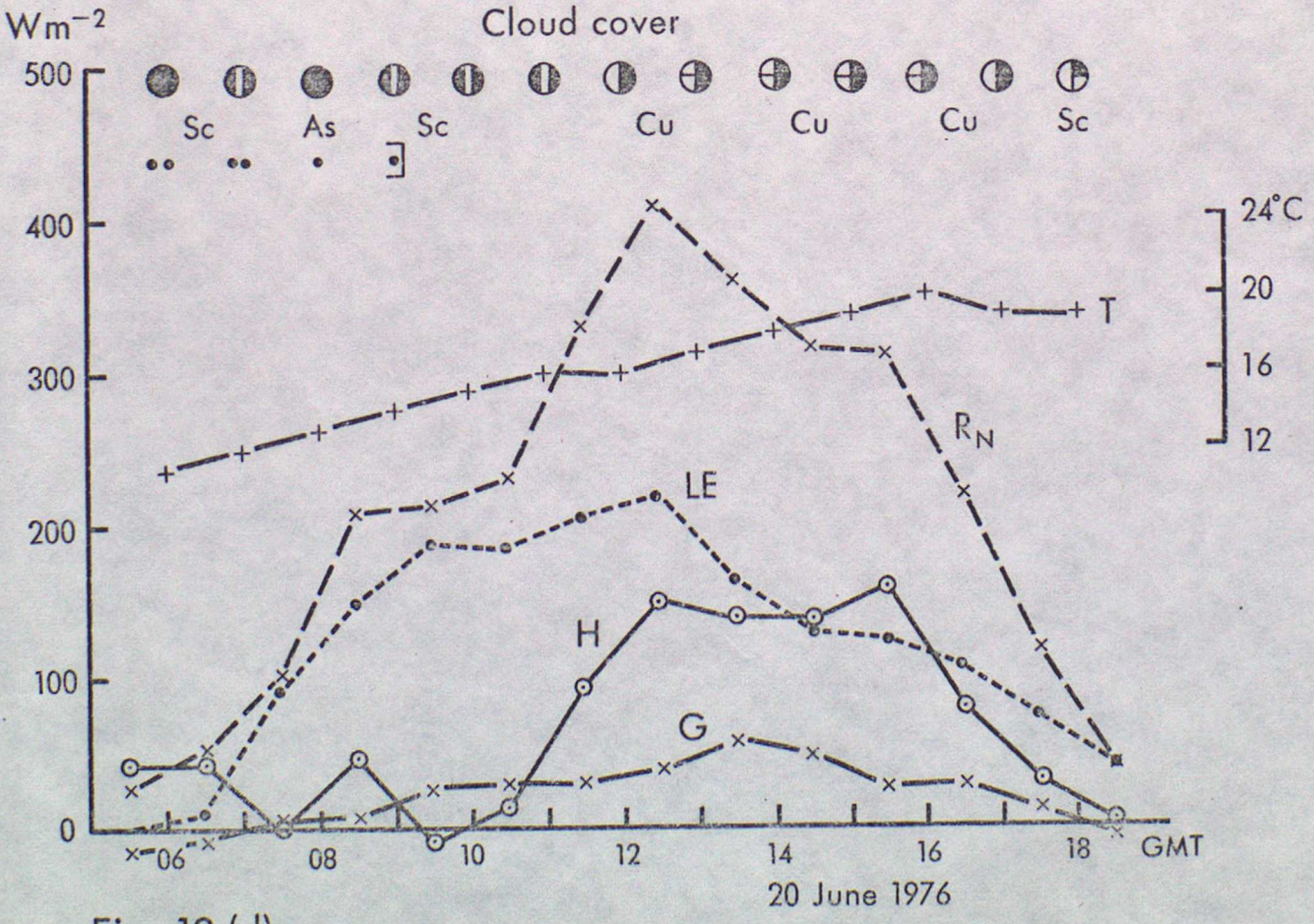

Fig. 12 (d)

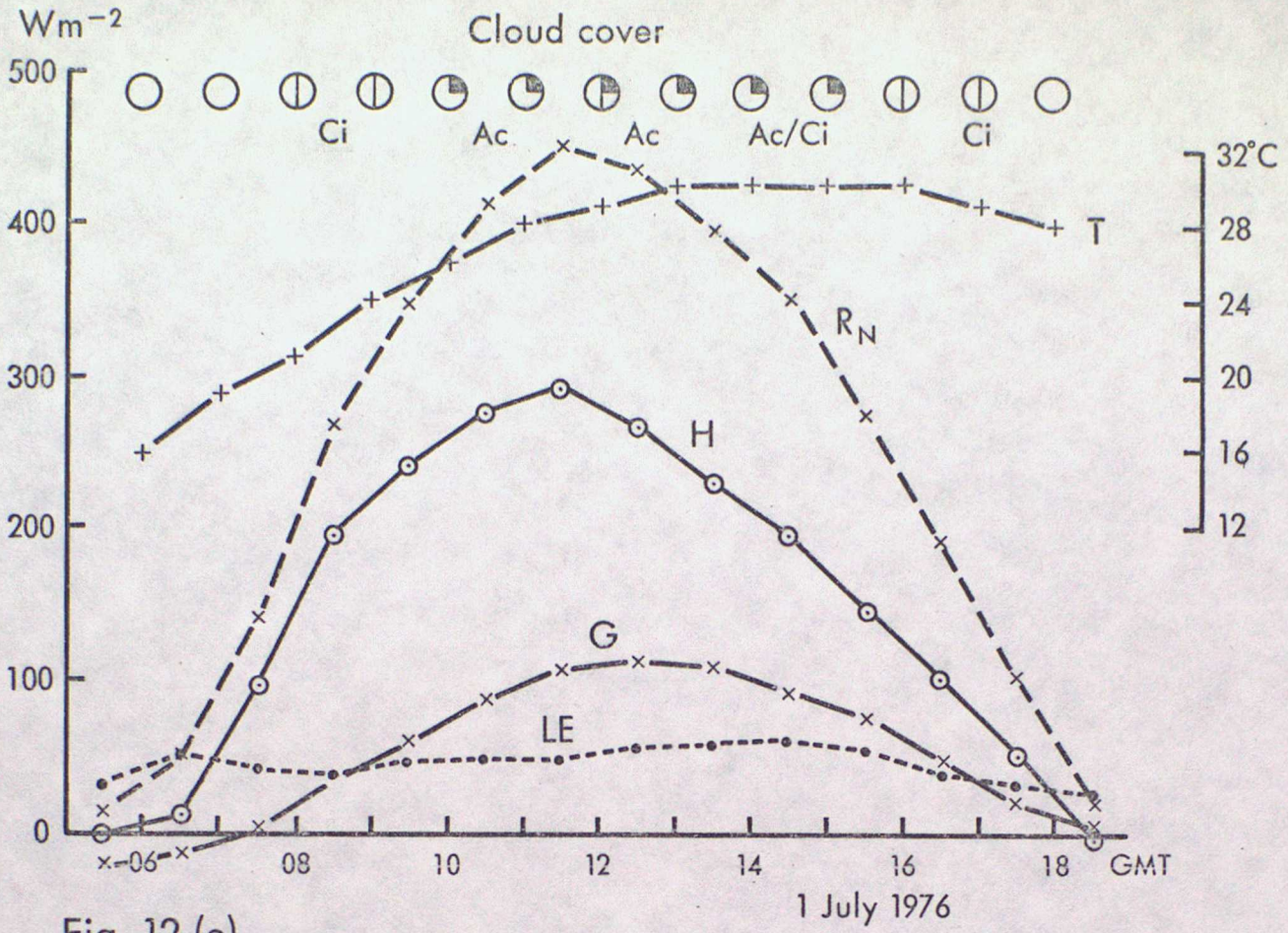

Fig. 12 (e)

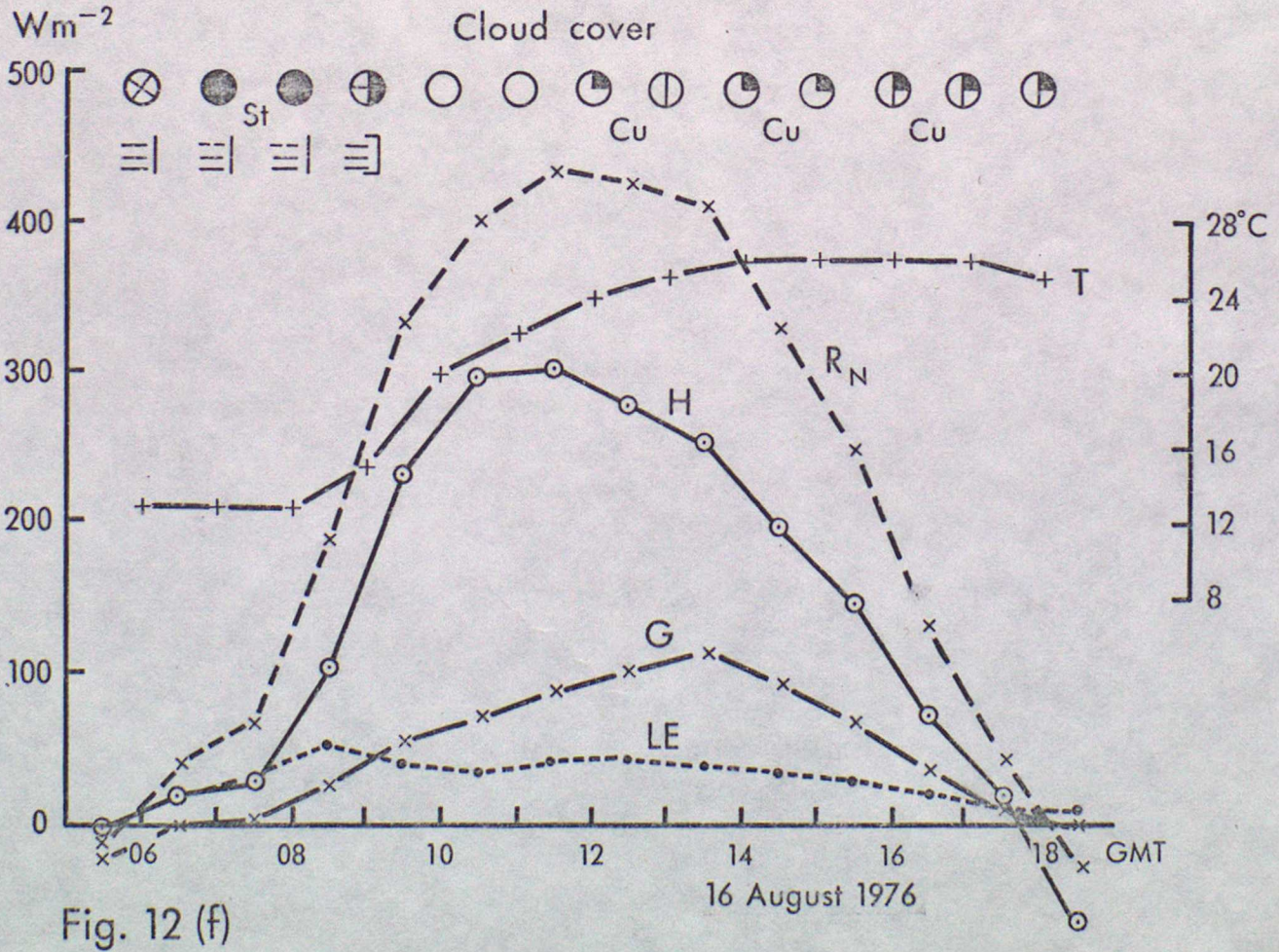

Fig. 12 (f)

1. Depth Z cm.	2. Az/A_5 percent	3. Diurnal Range measured Wm^{-2}	4. Diurnal Range predicted Wm^{-2}
0	156·8	145	122
5	100·0	78	78
10	63·8	54	50
20	26·0	17	20
40	4·3	3·6	3·4

Table 1. Comparison of the Actual Soil heat flux profile with the Theoretical Prediction